Korea-Australia Rheology Journal (2022) 34:223–238
https://doi.org/10.1007/s13367-022-00029-8

ORIGINAL ARTICLE

Impact of increased particle concentration on magnetorheological fluid properties and their damping performance

Ashok Kumar Kariganaur[1] · Hemantha Kumar[1] · M. Arun[1]

Received: 24 December 2021 / Revised: 4 April 2022 / Accepted: 11 April 2022 / Published online:11 May 2022

Abstract
Magnetorheological (MR) fluid properties are essential in analyzing the performance of any MR fluid system. The fluid properties are dependent on shape, size, and magnetic saturation of the magnetic particles. Preliminary characteristics with SEM, particle size analysis (PSA), and vibration sample magnetometer (VSM) on carbonyl iron particles were performed to verify the particle's feasibility to synthesize the MR fluid in a laboratory. Synthesis and characterization of MR fluids with particle concentrations (PC) of 10% (PC_{10}), 15% (PC_{15}), 20% (PC_{20}), 30% (PC_{30}), and 35% (PC_{35}) by volume are carried out. To show the inherent nonlinearity of the MR fluid, Herschel–Bulkley model is used. The relationship between sedimentation velocity, yield stress, and thermal conductivity is established as a function of particle concentration with experimental uncertainty of 6.15, 5, and 8.96%, respectively. Functional testing of PC_{15} and PC_{30} was carried out on an MR damper fabricated on dimensions obtained from the literature for the required size. The results indicate that damping force is 42% more in PC_{30} than PC_{15} at higher loading parameters. Finally, the saturation magnetization of the MR fluid depends not only on applied current but also on loading parameters when operating in the system.

Keywords Particle concentration · Sedimentation velocity · Thermal conductivity model · Uncertainty · Damper performance

List of Symbols

τ	Shear stress (Pa)
τ_H	Field (H)-dependent flow stress (Pa)
$\dot{\gamma}$	Rate of shear(s^{-1})
K	Consistency index
n	Flow behavior index
K_p	Particle thermal conductivity
K_f	Fluid thermal conductivity
ϕ	Particle concentration
N	Particle shape

1 Introduction

The properties of MR fluids change when subjected to an external magnetic field and regain their primary characteristics with the removal of the magnetic field. Because of this peculiar property, they are called "intelligent" fluids. Every constituent of MR fluid has its importance in the enhanced performance of the MR fluid system. The forces acting on the MR fluid while characterizations have their collective outcome on the behavior of the MR fluid. The essential properties that change with the application of an external magnetic field are suspension stability, dynamic yield stress, viscosity, and thermal conductivity, which mainly affect the dynamic behavior of the MR fluid system.

The properties of magnetic particles, such as shape, size, magnetic saturation, and viscosity, decide the yield stress, thermal conductivity, and sedimentation rate. Experiments prove that sedimentation rates can be minimized by coated particles and additives, stearic acid, fumed silica, and organoclay [3]. Some researchers evaluated that shapes, i.e., plate-like iron particles, flake-shaped particles, and bi-disperse particles, reduce the sedimentation rate by increasing the yield stress of the MR fluid [15, 23, 28, 32, 46, 49]. With octahedral-shaped magnetic particles as the additive, the rate of sedimentation and flow stress of the MR fluids can be enhanced [27]. MR fluids containing carbon nanotubes and iron oxide improve sedimentation stability [43]. When used in MR fluid preparation, cobalt magnetic particles give higher stability and magnetorheological properties than

✉ M. Arun
m.arun1978@gmail.com

[1] Department of Mechanical Engineering, National Institute of Technology Surathkal, Mangalore, India

carbonyl iron particles because of their higher magnetic saturation [14]. Moreover, plasma-treated and surface-modified (coating) magnetic particles with organic substances, gelatine, and graphite oxide increase sedimentation stability by decreasing the small amount of magnetic effect [8, 18, 41, 48]. Researchers have shown that using paraffin additive sedimentation can be drastically reduced compared to oleic acid, and the yield stress can be found with the limited chain model [54]. Silica-coated CI particles have a less rapid response time than pristine-coated CI particles, and also, there is less yield stress on pristine-coated particles [31]. If the particles are coated with polystyrene and multi-wall carbon nanotubes, the sedimentation of the fluid is enhanced, compromising the MR effect [16, 21]. Researchers proposed that the sedimentation in stages has direct impact on yield behavior of the MR fluid [30].

Apart from the particles' additive and coating, sedimentation can be reduced by increasing the particle concentration [6, 7, 56]. When prepared with wire-like iron nanoparticles along with the carbonyl iron, the MR fluids will significantly enhance the stability and magnetic properties, and an increase in nanoparticle concentration decreases the yield stress marginally [21, 22]. The increased particle concentration decreases the sedimentation rate with increased yield stress but gives rise to particle clumping, making the surface vulnerable to scratches [10, 24, 38, 53]. Different settling velocity models for various volume fractions of carbonyl iron particles were carried out through vertical axis inductance monitoring system [10]. Magnetorheological polishing fluids give abrasives and carbonyl iron particles [20]. Particle concentration and applied magnetic field raise the MR fluid's thermal conductivity [2, 17, 29, 55]. A practical model comparison has been proposed for temperature conductivity with concentration variation [37]. Particle size and interfacial shells also play an essential role in thermal conductivity value and particle concentration [35, 44]. The temperature conductivity of hybrid nanofluid can be improved by increasing the particle loading of magnesium oxide and nanotubes in ethylene glycol [42]. Brownian motion of nanoparticles in calculated quantities will enhance the temperature conductivity of the nanofluids [36]. Particle chain formation and defects in particles will impact the thermal conductivity determination of fluids [47]. The thermal conductivity of the compressed spacer fabric decreases with increased temperatures [39].

The essential parameters in the design of the MR damper are fluid gap, pole length, core length, number of coil turns, and external field supplied. The desired damping for an MR damper is found theoretically between the flow gap and the effective length [25, 50]. Later geometric dimensions for different valves are obtained through the ANSYS APDL approach, showing that the MR radial valve with two coils gives a better pressure drop and valve ratio [1, 33, 34].

Overall, the existing literature shows the effect of particle concentration on the flow properties of MR fluids. However, a study related to the model selection for sedimentation velocity for different concentrations, thermal conductivity, and damping performance of particle concentration in MR dampers is much needed. Hence, an effort was initiated to carry out this study to find the relationship between different carbonyl iron (CI) particle concentrations and critical fluid parameters, such as stability, yield stress, and thermal conductivity, with experimental uncertainty. To conclude, the damping performance analysis of PC_{15} and PC_{30} particle concentration was evaluated to comprehend the percentage increase in force at higher loading parameters.

2 Experimental study

Figure 1 shows the methodology flow chart followed for this study. Magnetorheological fluids were prepared using fork oil (manufacturer: Motul Fork Oil 20 W) as a carrier fluid and carbonyl iron powder as the suspension particles with a 2% carrier fluid additive (manufacture: Larson Calcium Base Grease). The particle size given by the manufacturers is 5–9 microns. For the study, PC10, PC_{15}, PC_{20}, PC_{30}, and PC_{35} by volume of CI particles (manufacturer: Sigma Aldrich, 44,890) of MR fluid samples have been prepared. Sedimentation stability is studied on a 10 ml glass measuring cylinder with 0.2 ml graduated markings. The characterization of the MR fluid was carried out on a Rheometer (manufacturer: Anton-Paar MCR502) to find the flow behavior of the fluid. The temperature conductivity of the MR sample with different particle loadings is tested on KD_2 pro equipment (manufacturer: Decagon devices), and the fork oil thermal conductivity is measured on liquid thermal conductivity apparatus for theoretical model analysis of thermal conductivity.

2.1 Sedimentation stability

Density dissimilarity between the particle and the base fluid creates a relative motion between them, making the particle settle to the bottom of the measuring cylinder. This is sedimentation, and the movement of the particle is hindered by buoyancy, resistance offered by the fluid, and interparticle friction.

$$\text{Sedimentation ratio} = \frac{\text{Height of clear fluid after settling (h)}}{\text{The total size of the MR fluid before deciding (H)}}$$

Particles are thoroughly stirred, and then the MR fluid sample is poured into the 10 ml vertical measuring cylinder with 0.2 ml graduations. Time taken for the settling of 0.2 ml was noted for all the volume samples. Changes in the

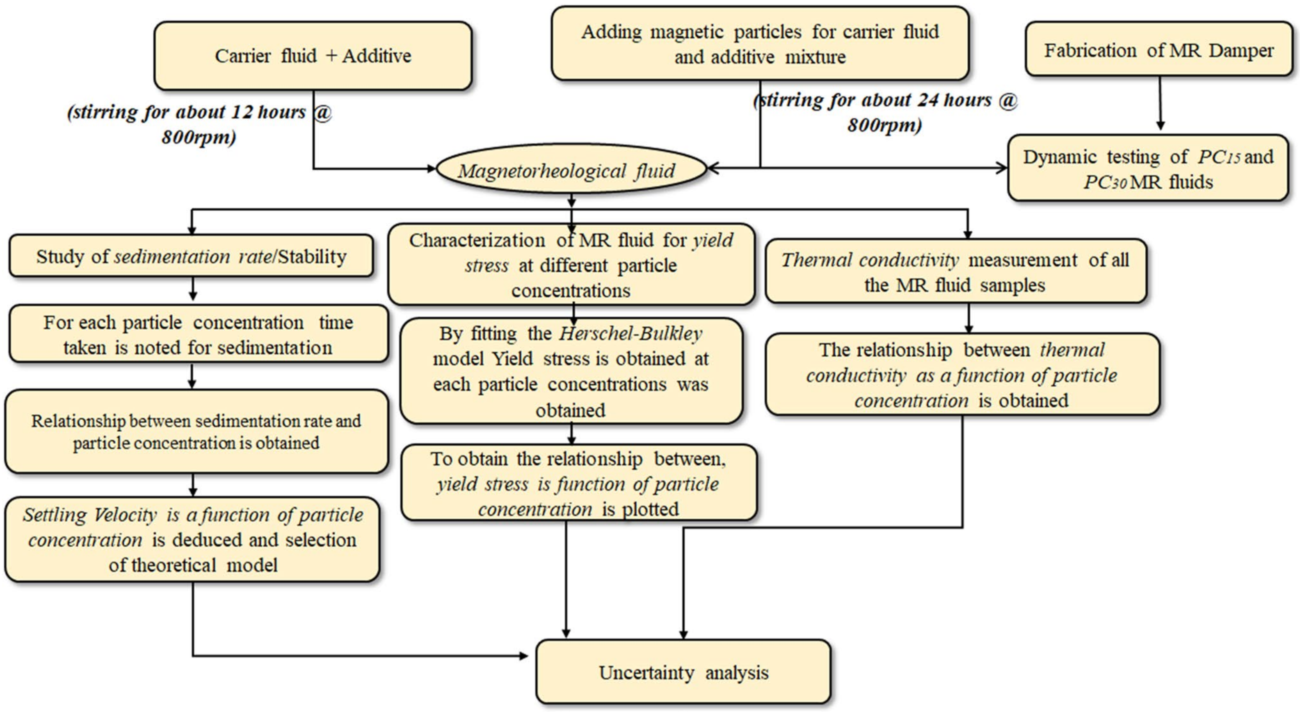

Fig. 1 Methodology flowchart

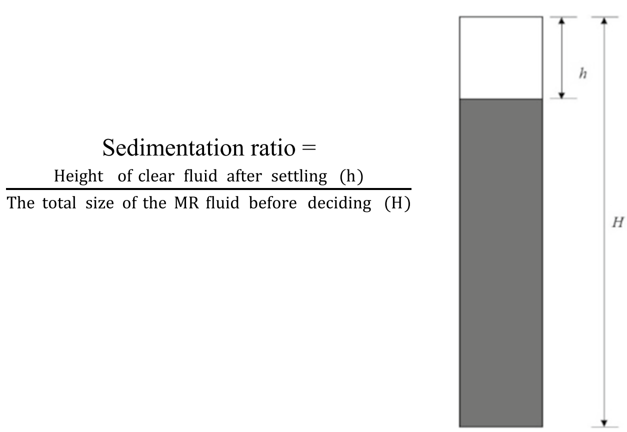

Fig. 2 Schematic diagram of sedimentation ratio

settling layer are investigated with time at room temperature. The settling velocity can also be deduced from the sedimentation rate depending upon the length to diameter ratio of the measuring tube. The schematic way of sedimentation is shown in (Fig. 2).

2.2 Rheology of MR fluid

The yield stress depends on the applied magnetic field and particle loading. The force between the two-particles decides the yield behavior of the MR sample up to the particular area, and it is validated through finite element modeling with that of the multipolar Klingenberg–Zukoski model [11, 23, 31]. The other essential parameters affecting the MR fluid's yield behavior are the magnetic field, particle size, and concentration. Rheometer (Anton-Paar MCR502) arrangement is used for flow characterization tests at zero (off-state) and 70KA/m (on-state) current with a 0.1 s^{-1} to 600 s^{-1} rate of shear. The MR fluid temperature was kept constant during the complete characterization of the sample with a water-cooled circulation bath. The parallel plate rheometer has a disk diameter of 20 mm in which the bottom plate is fixed while the top plate has a spindle attached to it rotating at the required speed, shearing the fluid between the plates maintained at a 1 mm gap. The increased magnetic flux intensity in the flow gap is achieved at the lower gap with higher currents. The effect of particle concentration is evaluated from tested results by comparing the yield stress at the 70KA/m current. The Herschel–Bulkley non-linear model is used to obtain the yield behavior of the fluid and is shown in Eq. 1.

$$\tau = \tau_H + K(\dot{\gamma})^n \quad (1)$$

$$\dot{\gamma} = 0, \tau < \tau_H$$

where τ = shear stress (Pa), τ_H = field (H)-dependent flow stress (Pa), $\dot{\gamma}$ = rate of shear (s^{-1}), K = consistency index and n = flow behavior index.

2.3 Magnetorheological fluid thermal conductivity

The thermal conductivity of the carrier fluid is measured separately in liquid thermal conductivity measuring equipment to calculate the theoretical model values to compare with experimental results and obtain a suitable model for MR fluid behavior. After analyzing the results, a relation for thermal conductivity in particle loadings is obtained. The thermal conductivity measuring equipment for carrier liquid is shown in (Fig. 3a). Different particle concentrations of thermal conductivity are obtained from KD_2 pro equipment shown in (Fig. 3b).

This section estimates the thermal conductivity of magnetic particles using experimental and theoretical models, such as Maxwell, Hamilton, and Bruggeman's.

Theoretical models for thermal conductivity is shown below:

Maxwell's model [44]

$$\frac{k}{k_f} = \frac{kp + 2k_f + 2\phi\left(kp - k_f\right)}{k_p + 2k_f - \phi\left(kp - k_f\right)} \tag{2}$$

K_p = particle thermal conductivity, K_f = fluid thermal conductivity, and ϕ = Particle concentration.

Hamilton–Crosser model

$$\frac{k}{k_f} = \frac{kp + (n-1)k_f - (n-1)\phi\left(k_f - kp\right)}{k_p + (n-1)K_f + \phi\left(k_f - k_p\right)} \tag{3}$$

where n depends on particle shape.

Bruggeman's model [26, 44]

$$\frac{k}{k_f} = \frac{1}{4}(3\phi - 1)\frac{k_p}{kf} + (2 - 3\phi) + \frac{K_f}{4}\sqrt{\Delta} \tag{4}$$

2.4 Testing of PC_{15} and PC_{30} in MR damper

A monotube shear mode magnetorheological damper performed dynamic testing of PC_{15} and PC_{30} particle concentrations. Table 1 shows the dimensions preferred for damper fabrication. After fabrication, it is fitted onto a damper testing machine (make: Heico Hydraulics and Engineering Instruments), which consists of two sensors: one position sensor fitted on top of the actuator to maintain the displacement of the piston, and a load cell at the bottom to measure the force obtained from the damper testing. Here, the MOOG controller is used in controlling the inputs of the damper. To estimate the damping force generated at different frequencies (1 Hz, 2 Hz, and 3 Hz) amplitudes (2 mm and 4 mm) and currents (0 A–1.2 A) for sinusoidal input displacement, (Fig. 4) shows the MR damper fitted onto the damper testing machine for characterization.

3 Results and discussion

3.1 Particle study

The morphology and size of the particles were studied on a SEM and PSA. The average particle size obtained through testing is 6.77 µm, and spherical shapes can be seen in (Fig. 5a, b). The size, shape, and particle concentration have an immense role in the fluid's stability,

Table 1 Damper geometric dimensions

Pole length	5 mm
Flow gap	1 mm
Core length	18 mm
Number of turns of the coil	300
Maximum operating current	1.5Amps

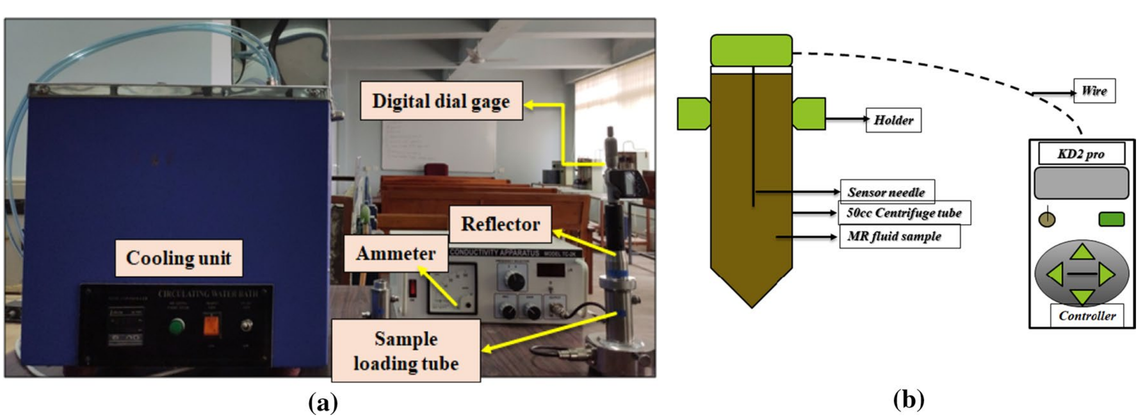

Fig. 3 **a** Liquid thermal conductivity equipment, **b** Schematic diagram of KD_2 pro thermal conductivity analyser for MR fluids

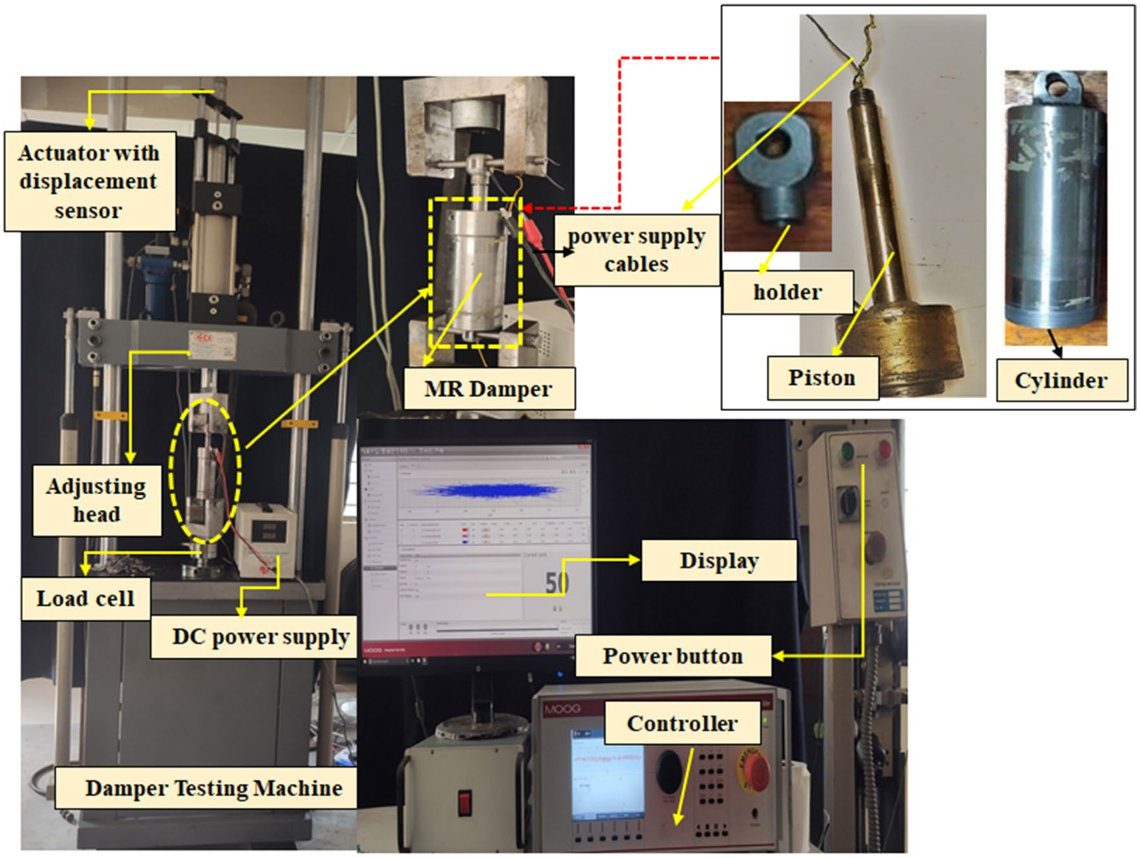

Fig. 4 Damper testing machine with MR damper

flow stress, and thermal conductivity. The sedimentation rate increases when particle size is larger because particle density is greater than carrier fluid density. The stability is also dependent on the particle shape, which is the particle's surface area. The magnetic saturation point of the particle will decrease at higher temperatures, and the particle with the higher magnetic saturation is selected for higher yield stress for MR fluid preparation. When the temperature effect comes into the picture, it plays a highly significant role as it affects all the constituents in the fluid. The magnetometer of the magnetic particles is carried out on a vibration sample magnetometer (manufacturer: lakeshore) at an atmospheric temperature between the ranges of $-12*10^3$ Gauss (G) and $+12*10^3$ Gauss which is shown in (Fig. 5c). The saturation value of the particles and MR fluid is 250 emu/g and 150 emu/g, respectively. A decrease in the saturation magnetization implies the effect of additive and carrier fluid, which act as a coating on the particles in homogenization. The retentivity and coercivity values of the particles and MR fluid are 0.15 emu/g, 0.57G, and 0.09 emu/g, 0.323, respectively.

3.2 Sedimentation ratio and velocity of the MR fluid samples

The sedimentation ratio is the ratio of the transparent carrier fluid zone directly above the particle layer to the overall volume of the fluid in the cylinder before settling. The general formula for calculating Stoke's velocity is given below:

$$\mathrm{v} = \mathrm{g} * \left(\rho_{\mathrm{p}} - \rho_{\mathrm{f}}\right) * \mathrm{d}^2/18\mu \tag{5}$$

Visually, the sedimentation ratio for all MR samples at ambient temperature is obtained. Figure. 6 shows the sedimentation of MR fluid samples of different particle concentrations. The time taken for the settling of particles is observed, and the sedimentation rate of the MR liquid layer is calculated. The compositions of MR fluids are given in Table 2.

In this study, sedimentation velocity of MR fluids is measured experimentally with varying particle concentrations to evaluate the nearest theoretical settling model for better understanding of settling mechanism involved in the MR fluids. Sedimentation is the time-dependent deposition

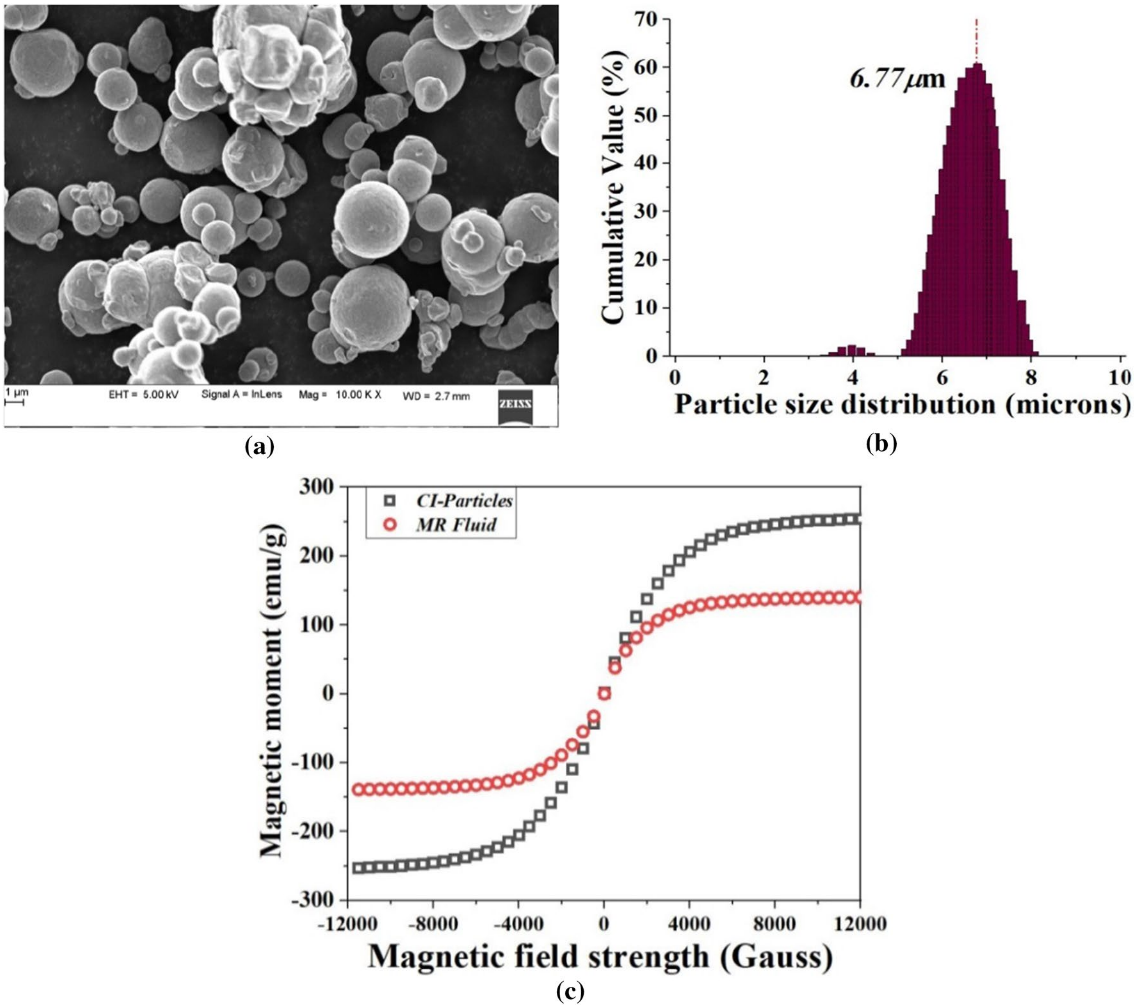

Fig. 5 **a** SEM image of CI particles, **b** Particle size distribution, **c** VSM of CI particles and MR fluid

of particles due to density difference between carrier fluids and CI particles. For lower dispersions, Stoke's settling law is used to calculate the terminal velocity of a particle [4, 19]. As for the particle concentration, increased settling rate and fluctuations in the settling velocities of the particles reduce due to the interparticle interactions and restriction of particle movement as the interparticle distances become shorter which also increases the fluctuations in the sedimentation [10, 40]. A particle settling in the batch of particles experiences a hindered settling, also due to the drag force exerted by the fluid flow and the particle–particle interactions. Subsequently, it reduces the mean settling velocity of the suspension with respect to the terminal velocity of a single particle. To study the higher concentration of particles settling, some of the models were explained in detail below [4, 45, 51, 57]

Richardson–Zaki model

$$V\varphi = Vp * (1 - \varphi)\,n \tag{6}$$

$$n = 2.35(2 + 0.175Re3/4)/(1 + 0.175Re3/4) \tag{7}$$

$$Re = (\rho f * Vp * \mu)/dp \tag{8}$$

where V_p = velocity of dilute particles (m/s), n = constant, and Re = Reynolds number, d_p = diameter of the particle (m), φ = particle concentration (%), ρ_f = density of the carrier fluid (kg/m3), μ = viscosity of the fluid (Pa-s).

Steinour model

$$V\varphi = Vp * (1 - \varphi)2 * 10 - 1.82\varphi \tag{9}$$

Batchelor model

$$V\varphi = Vp * (1 - n\varphi) \tag{10}$$

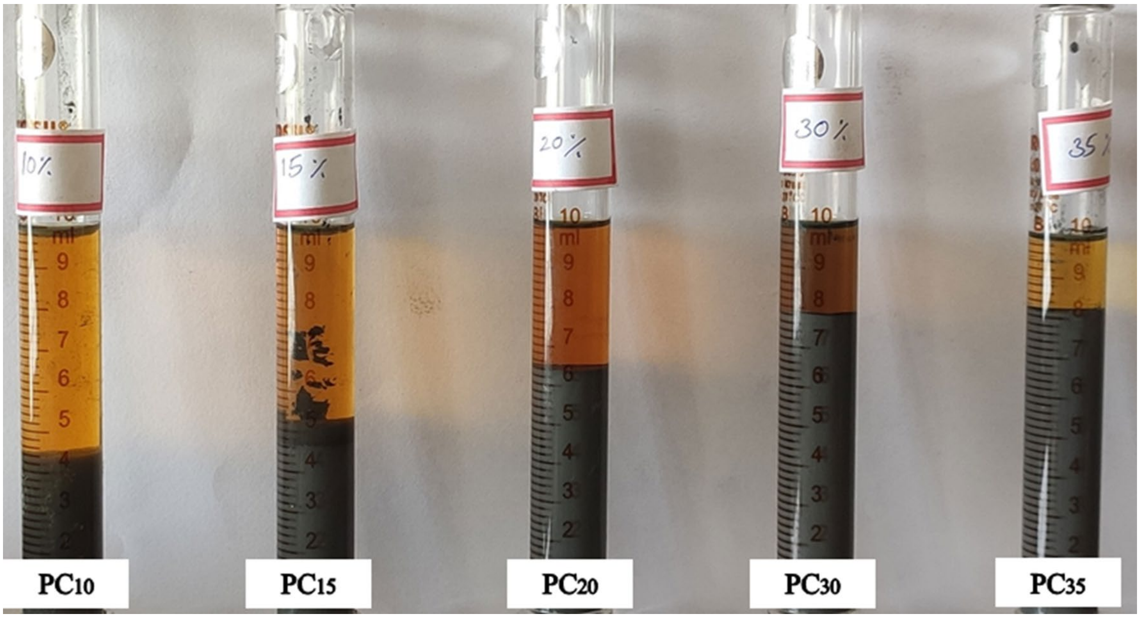

Fig. 6 Stability analysis of different particle concentration MR fluid samples

Table 2 MR fluid compositions with fork oil as carrier fluid

Sample name	Particle concentration by volume (%)	Additive percentage by weight (%)
PC_{10}	10	2
PC_{15}	15	2
PC_{20}	20	2
PC_{30}	30	2
PC_{35}	35	2

Vesilind model

$$V\varphi = Vp * e - n\,\varphi \tag{11}$$

Dick model

$$V\varphi = Vp * \varphi n \tag{12}$$

The sedimentation rate is important at initial regions compared to later regions. This might be due to particle aggregation and frictional forces at the later regions after a certain time. The sedimentation behavior of all MR fluid samples is quite the same. There is a decrease in sedimentation rate with the period as the mean path between the particles lessens, instigating more and more particle connections. For PC_{10} volume concentration, the rate at which the particle interface layer travels is 0.17 μm/s, and it takes 240 h to settle completely at 58%. And for PC_{15} concentration, the sedimentation rate is 0.125 μm/s and it takes 198 h approximately to settle completely at 48%. The reduction in sedimentation rate from PC_{10} to PC_{15} particle concentration is 26.4%, and the settled fraction is 10% less than the PC_{10} volume fraction. For PC_{20}, PC30, and PC_{35} concentrations, the sedimentation rates were 0.0575 μm/s, 0.02 μm/s and 0.009 μm/s and it took 152 h, 112 h, and 70 h to settle completely at 36, 23, and 19%, respectively. When particle concentration increases from PC_{20} to PC30, there is a 65.2% decrease in sedimentation rate compared to PC_{10} to PC_{15} concentrations, and for PC_{20} to PC_{35}, there is an 84.34% decrease in the sedimentation rate. From PC_{10} to PC_{35} volume fraction, there is a 94.71% decrease in the sedimentation rate, which is highly significant in terms of the stability of the MR fluids. From the analysis, it is apparent that more particle concentration decreases the rate of sedimentation, which is very much needed for MR fluid applications. Nonetheless, increasing particle concentrations make fluids viscous, resulting in difficult-to-disperse agglomerations. Also, the time taken for dispersibility is greater after complete settling.

Figure 7 shows the thickness of different particle concentrations of MR fluids. It can be observed that at PC_{10} there is no agglomeration of particles compared to PC_{35}, where there is an enormous packing of particles that makes dispersing difficult after settling, which hinders the performance of the fluid system by sticking on to the surfaces of the system.

The curve fit analysis in (Fig. 8a) shows that the sedimentation rate decreases exponentially ($r^2 = 0.978$). The theoretical model analysis shows Vesilind and Dick's model is close to the testing results. The Richardson–Zaki, Steinour, and Batchelor models can be further studied for lower volume

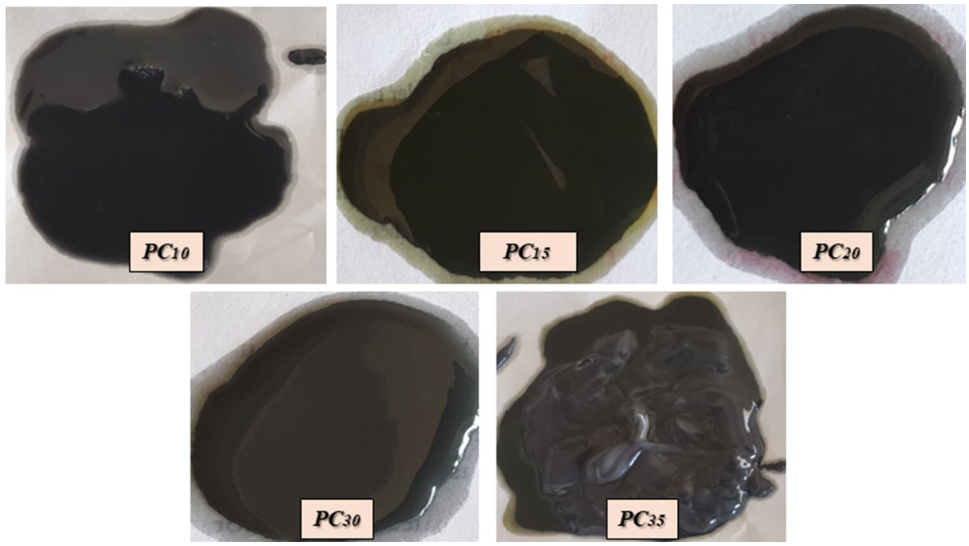

Fig. 7 Different particle concentrations

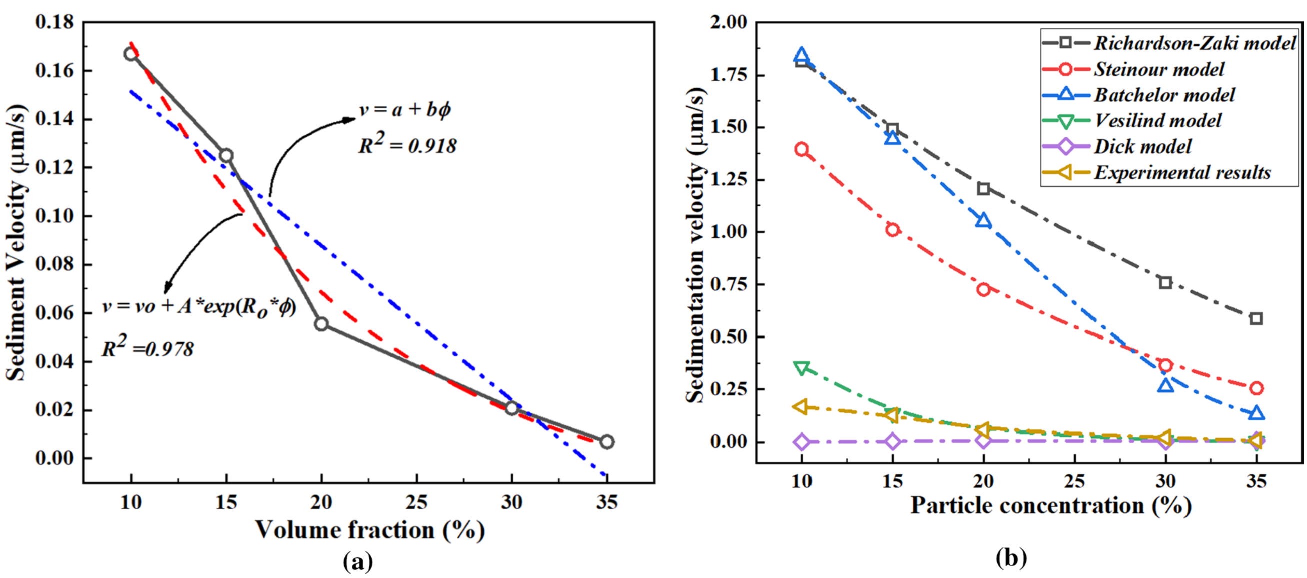

Fig. 8 **a** Sedimentation velocity versus particle concentrations, **b** model comparisons of the sedimentation velocities with experimental tests

fraction compositions. The different model plots are shown in (Fig. 9b).

3.3 Yield stress of the MR fluid

The performance of any MR fluid system depends on the MR fluid's yield stress. The yield stress can be increased by adding a larger particle size, higher particle concentration, higher magnetic fields, lower temperatures, and selecting a particle with a higher magnetic saturation point. This effect of particle concentration on yield stress is obtained at a single current to see the variation in yield stress. In the particle study section, it was briefly explained about the effects of particle size, shape, and concentration. Still, researchers proved that the cobalt nanofibres have a higher saturation magnetization point. The flow properties of MR fluids are measured at 0A and 2A currents to study the variation in yield stress concerning particle loading. (Fig. 8a, b) presents the shear stress behavior concerning shear rate. Figure 10 shows the variation in yield stress of the MR fluid at various particle loadings. At PC_{10}–PC_{15} particle concentrations, the yield stress measured is 2060 Pa and 3159 Pa, respectively, 53.35% higher than the latter. At PC_{20}, yield stress is approximately 4000 Pa, which is 26.61% higher than 15%, and between PC_{20} and PC_{30}, there is an increase of 42.5% yield stress, and at PC_{35} particle concentration, it is 15.44% higher yield stress compared to PC_{30} particle concentration. The average increase in yield stress is 34.475%

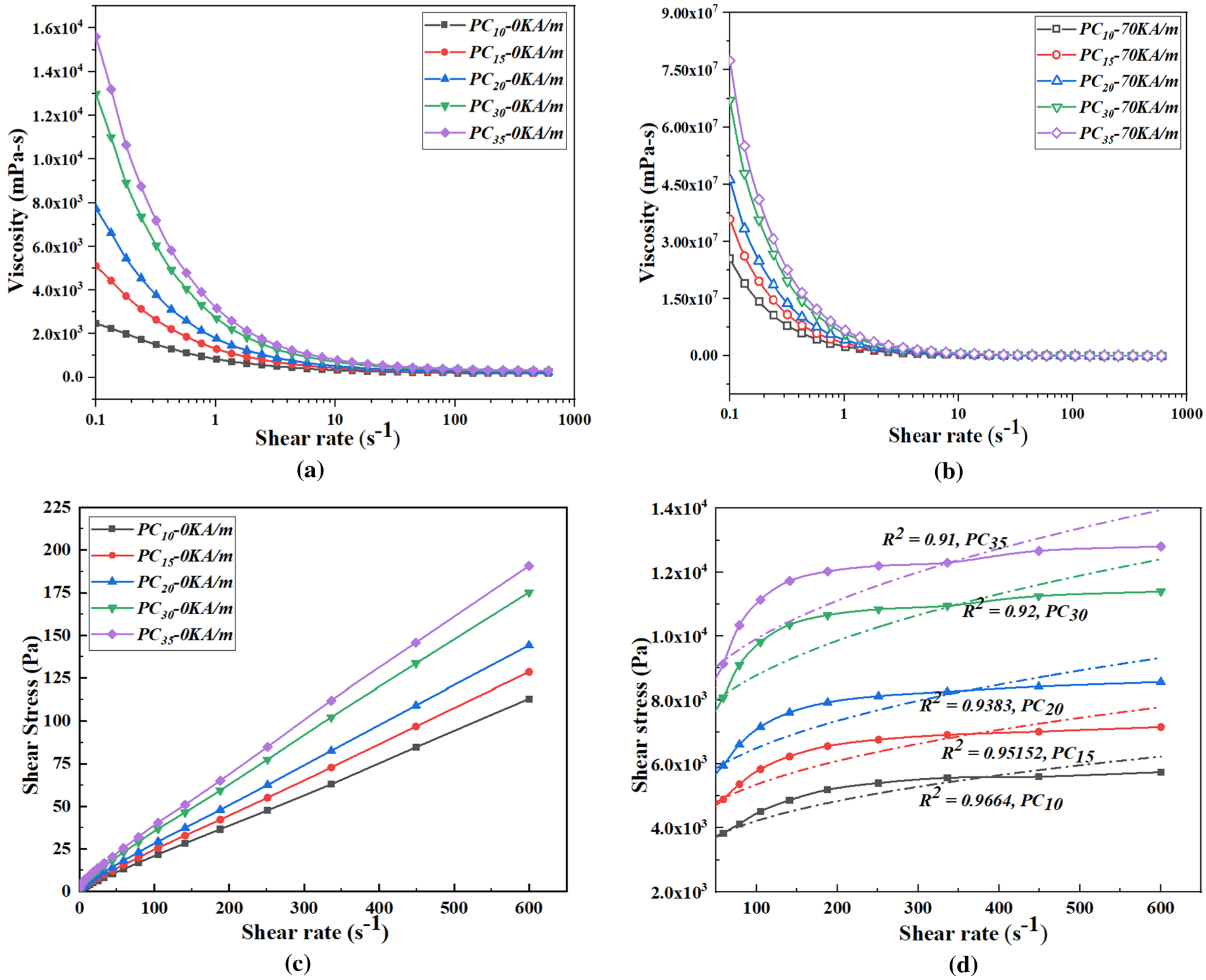

Fig. 9 (**a**–**d**) Flow curves at zero and 70KA/m KA/m and HB-Model Fit

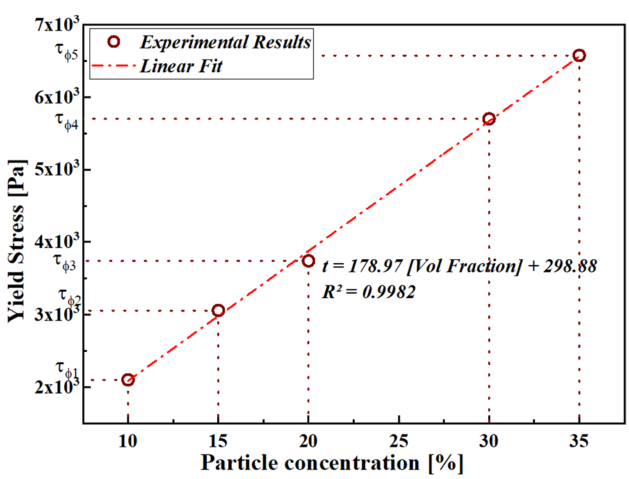

Fig. 10 Variation in yield stress with particle concentration

for every 5% increase in particle concentration in the MR fluid sample. The percentage variation in yield stress might be due to the difference in the MR sample's concentration for testing, consisting of different size ranges of particles and differences in sample loading. The above analysis shows that increased particle concentration leads to a linear increase in yield stress.

The shear stress curve for different volume fractions at zero and 70KA/m is shown in (Fig. 8a, b). Shear stress of the MR fluid is dependent on particle size, volume concentration, and applied magnetic field. (Fig. 8a, b) shows that increase in particle concentration increases the shear stress along with the increased yield stress of the fluid due to more chains formation. The particle size range used for this study is 5–9 microns. As the particle concentration and shear rate increase, the MR fluid performance improves. The performance improvement is higher with particle size range of 5–9 microns than particles of smaller particles sizes [9, 23, 46]. In the process of chain formation, the smaller particle comes in contact between the two larger particles, and at high shear rate, the smaller size particles in the chains disrupt the further increase of shear stress than nonlinear model fit curve shown in (Fig. 8d). It is interesting to note from the figures that at higher shear rate, MR fluid is unable to provide higher shear stress particle chains due to the shear thinning effect of the fluid [5, 12, 18, 52]. MR fluid with moderate particle fractions iron particles is a good option at low to moderate shear rate.

3.4 Magnetorheological fluid thermal conductivity

The importance of thermal conductivity in MR fluid is to dissipate heat from the system to the ambient if the system is operating for a prolonged period of time making the fluid temperature rise. Figure 10a, b bshows the thermal conductivity for particle concentration. At the peak concentration of particles (PC_{35}), the thermal conductivity is 2.5 times greater than the initial concentration (PC_{10}). The enhanced particle loadings and magnetic field lead to an upsurge in the thermal conductivity and viscosity of the fluid. Many researchers show that enhancement in thermal conductivity depends on particle concentration, size, shape, and the type of base fluid, but the theoretical model for MR fluid has less literature. Table 3 shows the theoretical model and error analysis between the experimental and three thermal conductivity models. The linear fit for the thermal conductivity of MR fluids is articulated in Eq. 13 within the chosen particle concentrations.

$$K = 0.0093 * \varphi + 0.0741;\ 10\,\% < \varphi < 35\% \tag{13}$$

There is not much practical application for lower volume fractions in MR fluids, and it is proved by research that there is no linearity in thermal conductivity and particle loadings. Figure 10a gives us the linear curve fit analysis for thermal conductivity with $R^2 = 0.967$ and (Fig. 10b) gives us the thermal conductivity model comparisons. The average error associated with Maxwell's model is 5.77%, the average error related to the Hamilton–Crosser model is 7.2835%, and Bruggeman's model is 20.586%, respectively. The trend followed by Maxwell's model is also linear, which can be related to the experimental linear fit.

Table 3 Error analysis of different models with experimental results

Particle concentration (%)	Relative error between experimental and Maxwell's model (%)	Relative error between experimental and Hamilton Crosser model (%)	Relative error between experimental and Bruggeman's model (%)
PC_{10}	4.7619	2.3385	0.4862
PC_{15}	3.8437	1.3935	7.9041
PC_{20}	6.5333	2.1798	12.2399
PC_{30}	5.9744	12.9841	43.6995
PC_{35}	7.7405	17.5217	38.5989

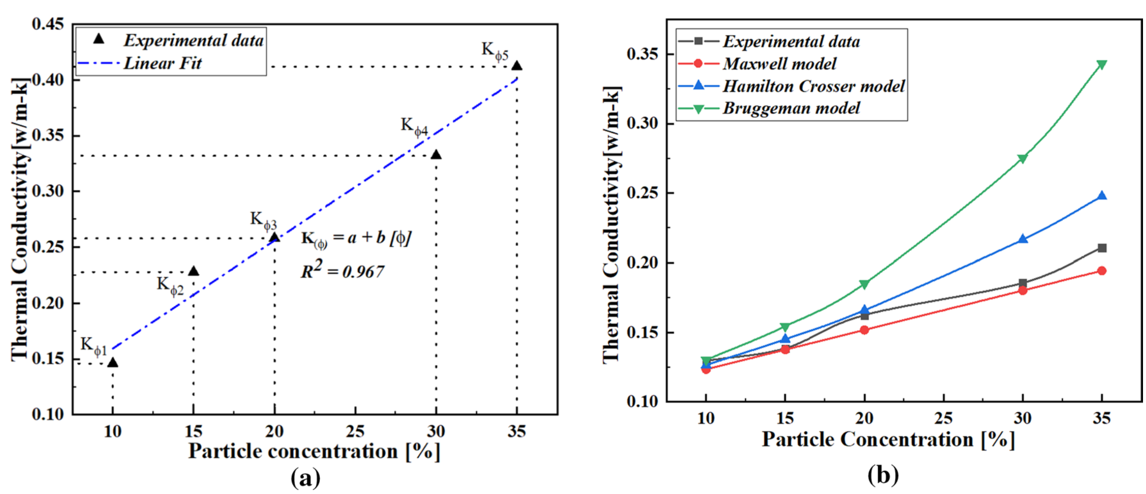

Fig. 11 **a** Thermal conductivity as a function of particle concentration, **b** Experimental and theoretical model comparisons

4 Uncertainty associated with the experimentation

Uncertainty in any experimentation is possible from many sources, which are exhaustive in the study. Still, there might be variations in measuring quantity, particle size, atmospheric conditions, errors associated with equipment, etc. Uncertainty evaluation implies increased confidence in the validity of experimentation. The components and other associated variables are obtained from standard deviations.

The overall uncertainty of the experiments can be obtained as:

$$\frac{dU}{U} = \sqrt{\left(\frac{dv^2}{v}\right) + \left(\frac{d\tau^2}{\tau}\right) + \left(\frac{dk^2}{k}\right)} \tag{14}$$

where U is the uncertainty, v is the settling velocity, τ is yield stress, and K is the thermal conductivity.

Each of the uncertainties has been analyzed individually. Generally, the uncertainty of the present measurement lies between 6.15% for sedimentation velocity, 5% for yield stress, and 8.96% for thermal conductivity.

5 Dynamic test results of PC_{15} and PC_{30}

The sinusoidal input displacement amplitude is varied from 2 to 4 mm and the frequency is 1 Hz–3 Hz at 0A, 0.3A, 0.6A, 0.9A, and 1.2A. The force–displacement plots for different frequencies at different currents are shown in (Figs. 12, 13). The distortion of the force–displacement graph can be explained by coulomb damping at a lower and higher frequency of operation [13]. This section gives us the results and observations made after the result analysis. The increase in the area of the force–displacement plot is increased with applied currents. This increase in the size of the plot is up to the threshold value, which is the saturation point of the MR fluid beyond, which there is no increase in the damping force and the damping force remains constant. An increase in the size of the loop indicates more energy dissipation into the fluid. Figure 12a–f shows that there is little difference between the two concentrations at 2 mm amplitude, 1 Hz frequency, and 0 A, which have roughly the same forces (60 N). At 1.2 A, there is an increase in the damping force of 118.42 N to 168 N from PC_{15} to PC_{30} volume concentration of particles. At 2 mm amplitude, 2 Hz frequency, and 0 A, there is a 76.2 N to 118.42 N force increase, and at 1.2 A, force is increased from 134.1 N to 186 N. For the sample, with 2 mm amplitude and 3 Hz frequency, at 0A, force increases from 92 to 157 N, and at 1.2A, force increases from 156 to 212 N. The rise in damping force means that there will be more chain formation, increasing the resistance to the movement of any solid surface. Figure. 13a–f shows that at 4 mm amplitude and 1 Hz frequencies, force increases from 84 to 122 N and 146 N to 196 N, respectively, at 0A and 1.2A. At 2 Hz frequency, the 129 N force is increased to 189 N for 4 mm amplitude and 0A current, and at 1.2A current, there is not much increase in force, i.e., from 189 to 193 N. At 4 mm amplitude and 3 Hz frequencies at 0A and 1.2A currents, there is not much rise force, indicating the saturation point of the MR fluid. The increase in amplitude at a particular frequency and current increases the damping force, i.e., for PC_{15} at 2 mm amplitude and 1 Hz frequency, the force obtained at 1.2A was 118.42 N and at the same 1 Hz frequency, the 4 mm amplitude at 1.2A force obtained was 146 N. Also, at particular amplitude and varying frequency, there is an increase in the damping force, i.e., for PC_{15} volume fraction at 2 mm amplitude, 1.2A current at 1 Hz and 2 Hz frequency, the force obtained was 118.42 N and 136 N, respectively. At the same 2 mm amplitude, 1.2A at 1 Hz and 3 Hz frequency, the forces obtained were 118.42 N and 156 N, respectively. The shift in the force-displacement curve is due to the absence of an accumulator in the damper, which compensates for the piston rod volume fluid displacement. Figure. 14a, b shows the damping force dependence on amplitude, frequency, and current.

6 Conclusion

1. The preliminary particle analysis observed that particles are spherical with an average particle diameter of 6.77 µm and feasible saturation magnetization, suitable for MR fluid preparation.
2. The observations were made to evaluate sedimentation results. (1) An increase in particle concentration decreases the sedimentation rate due to the particle–particle interaction. (2) The second observation is that the decrease in sedimentation rate follows an exponential drop with $R^2 = 0.978$ for an increase in particle concentration. (3) From the theoretical model analysis, it can be concluded that the Dick model is very well suited for the MR fluid settling analysis for higher particle concentrations with lower error than other models.
3. The yield stress is an essential parameter in deciding the performance of any system employed with MR fluids. Here, an increase in particle concentration increases the yield stress linearly. When particle concentration increases from PC_{10} to PC_{35} in the absence of a magnetic field, yield stress increases six fold, while yield stress increases threefold at 2 amps of current.
4. Changes in the various input parameters make MR fluid thermal conductivity vital for the long-term operation of the MR system. The thermal conductivity

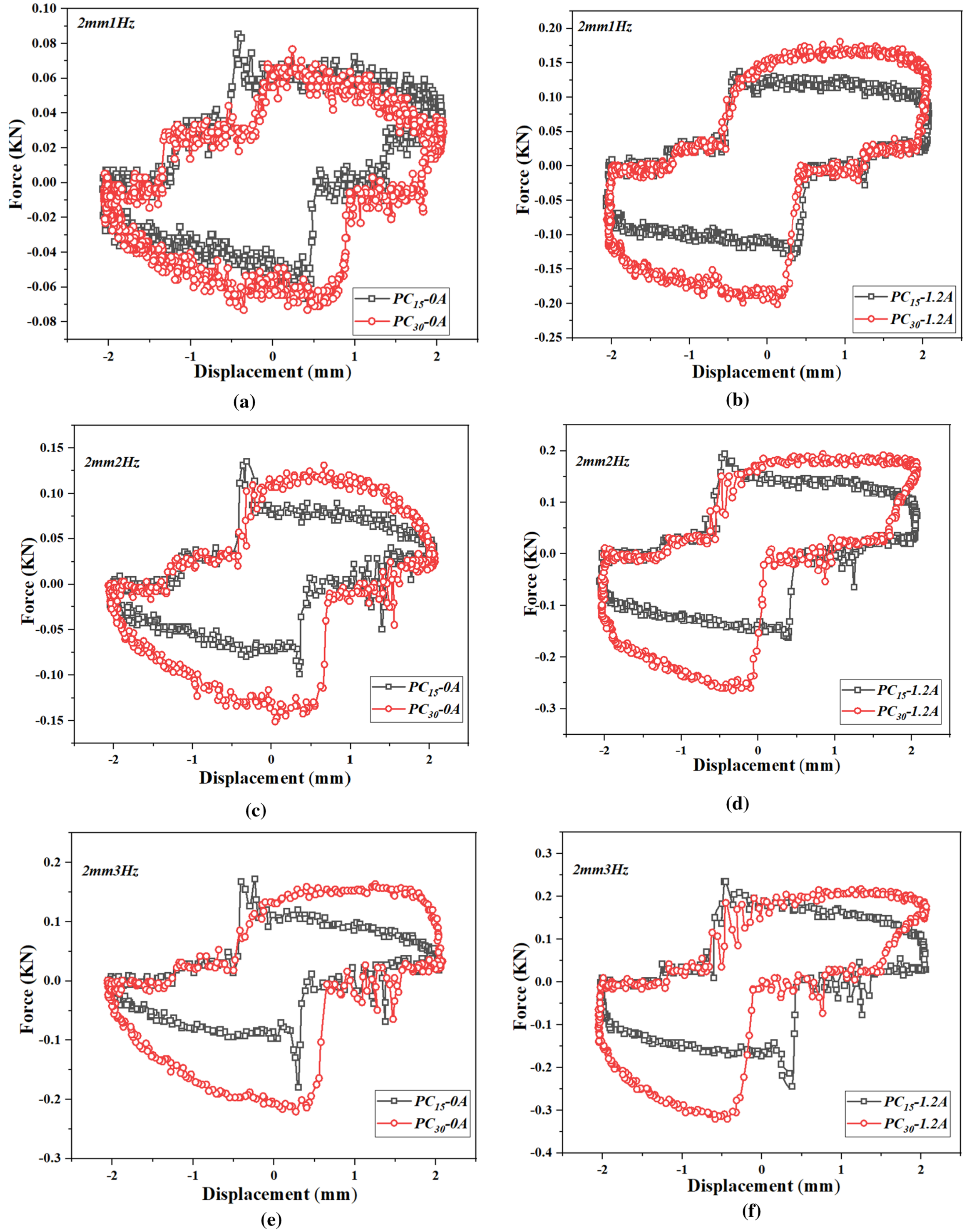

Fig. 12 (**a**–**f**) Damping characteristics at 2 mm amplitude and 1 Hz, 2 Hz, and 3 Hz frequency, respectively

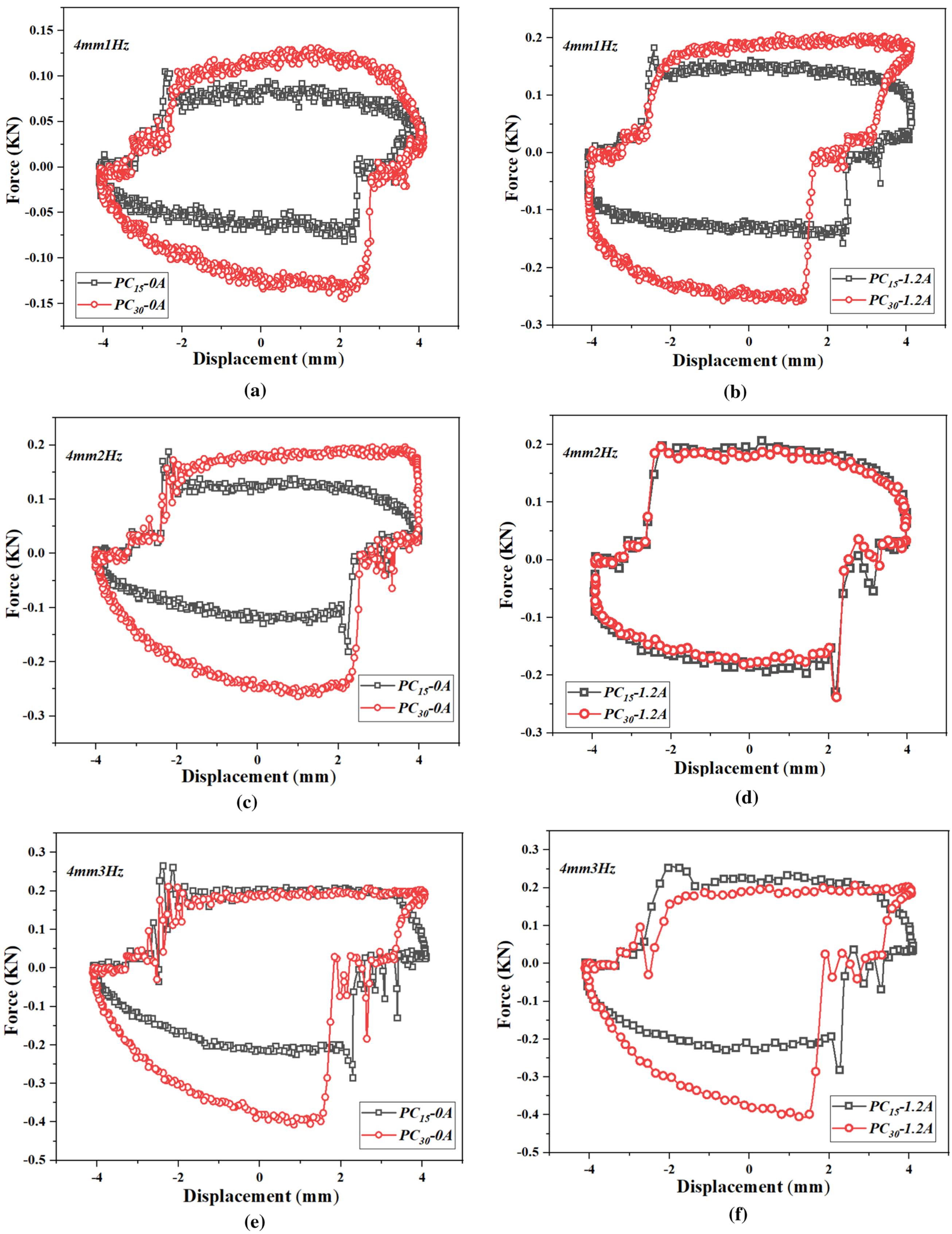

Fig. 13 (**a**–**f**) Damping characteristics at 4 mm amplitude and 1 Hz,2 Hz, and 3 Hz frequency, respectively

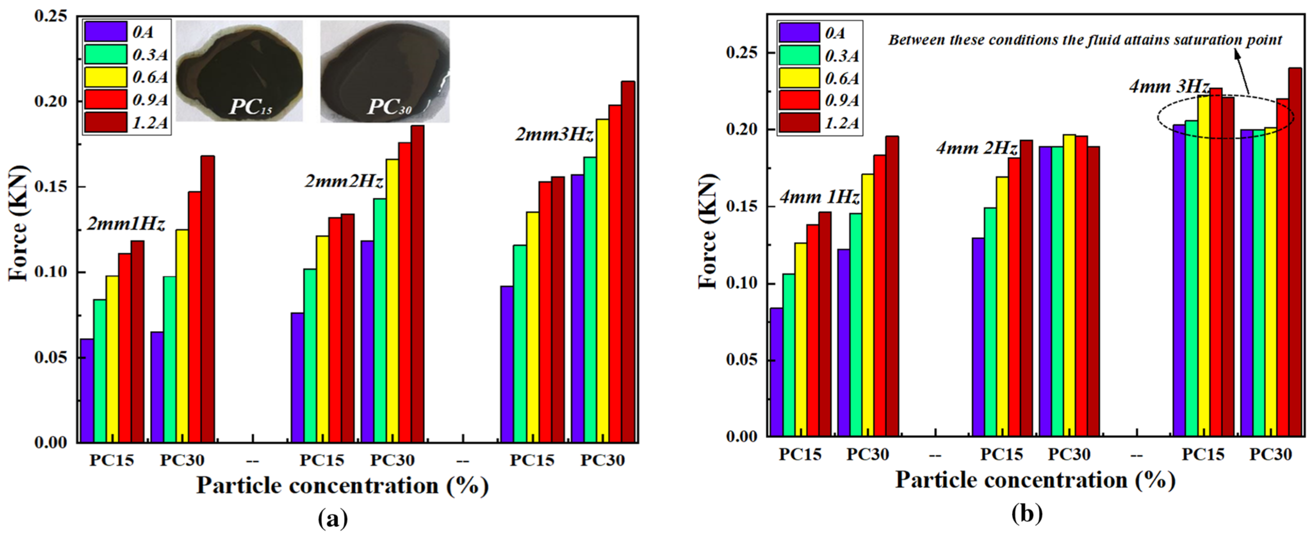

Fig. 14 Force versus Particle concentrations

study shows a linear gradient with increased particle concentration. From the theoretical model analysis, Maxwell's model can be applied for MR fluid thermal conductivity analysis with an average error of 5.77% compared to other models.

5. The reliability of the experimental analysis was calculated through uncertainty, and the total uncertainty associated with experimentation was 12.02%.
6. The conclusions from the performance analysis of the MR fluids are as follows:
   (i) The force obtained at particular amplitude, frequency, and current (i.e., 2 mm, 1 Hz, and 1.2A) is 42% more in the case of PC_{30} than PC_{15}.
   (ii) At a particular frequency of 1 Hz, the force obtained at 1.2A current, 2 mm amplitude at PC_{15} particle loading is 23% less than at 4 mm at 1.2A current. And at the same frequency, 1 Hz, and the force obtained at 2 mm amplitude, 1.2A current at PC_{30} volume concentration is 16.67% less than that of 4 mm amplitude and 1 Hz frequency.
   (iii) At specific amplitude of 2 mm, the force obtained at a 1 Hz frequency is 31.84% less than the 3 Hz frequency for PC_{15} volume fraction. And at PC_{30} volume concentration, the force obtained at 1 Hz is 31.45% less than that of the 3 Hz frequency at 2 mm and 1.2A. Overall, the force can be increased in the decreasing order of amplitude, frequency, and applied current.
   (iv) Along with the applied magnetic field, the saturation magnetization of the MR fluid is dependent on the loading factors. If the input parameters, i.e., amplitude, frequency, and currents, are higher, the saturation of the fluid is attained at an early stage.

Acknowledgements The authors acknowledge the Ministry of Human Resource Development and Ministry of Road Transport and Highways, Government of India, supporting this research through IMPRINT Project Fund No. IMPRINT/2016/7330 titled "Development of Cost-Effective Magnetorheological (MR.) Fluid Damper in Two wheelers and Four Wheelers Automobile to Improve Ride Comfort and Stability."

Declarations

Conflict of interest The authors declare that there is no conflict of interest.

References

1. Abd Fatah AY, Mazlan SA, Koga T et al (2015) A review of design and modeling of magnetorheological valve. Int J Mod Phys B 29:1530004
2. Afrand M (2017) Experimental study on thermal conductivity of ethylene glycol containing hybrid nano-additives and development of a new correlation. Appl Therm Eng 110:1111–1119
3. Ashtiani M, Hashemabadi SH, Ghaffari A (2015) A review on the magnetorheological fluid preparation and stabilization. J Magn Magn Mater 374:711–715
4. Batchelor GK (1972) Sedimentation in a dilute dispersion of spheres. J. Fluid Mech 52:245–268
5. Becnel AC, Hu W, Wereley NM (2012) Measurement of magnetorheological fluid properties at shear rates of up to 25000 s -1. IEEE Trans Magn 48:3525–3528. https://doi.org/10.1109/TMAG.2012.2207707
6. Bica I, Anitas EM, Averis LME, Bunoiu M (2015) Magnetodielectric effects in composite materials based on paraffin, carbonyl iron and graphene. J Ind Eng Chem 21:1323–1327
7. Bossis G, Volkova O, Grasselli Y, Ciffreo A (2019) The role of volume fraction and additives on the rheology of suspensions of micron-sized iron particles. Front Mater. https://doi.org/10.3389/fmats.2019.00004

8. Cheng H, Wang M, Liu C, Wereley NM (2018) Improving sedimentation stability of magnetorheological fluids using an organic molecular particle coating. Smart Mater Struct 27:075030
9. Chiriac H, Stoian G (2010) Influence of particle size distributions on magnetorheological fluid performances. In: J Phys: Confe Ser. Institute of Physics Publishing 200:072095
10. Choi Y-T, Xie L, Wereley NM (2016) Testing and analysis of magnetorheological fluid sedimentation in a column using a vertical axis inductance monitoring system. Smart Mater Struct 25:04LT01
11. De Vicente J, Klingenberg DJ, Hidalgo-Alvarez R (2011) Magnetorheological fluids: a review. Soft Matter 7:3701–3710
12. de Vicente J, Vereda F, Segovia-Gutiérrez JP et al (2010) Effect of particle shape in magnetorheology. J Rheol (N Y N Y) 54:1337–1362. https://doi.org/10.1122/1.3479045
13. Desai RM, Jamadar MEH, Kumar H et al (2019) Design and experimental characterization of a twin-tube MR damper for a passenger van. J Brazilian Soc Mech Sci Eng 41:332
14. Dong X, Tong Y, Ma N et al (2015) Properties of cobalt nanofiber-based magnetorheological fluids. RSC Adv 5:13958–13963
15. Ekwebelam C, See H (2009) Microstructural investigations of the yielding behaviour of bidisperse magnetorheological fluids. Rheol Acta 48:19–32
16. Feng Z (2015) Study of sedimentation stability of magnetorheological fluid. Adv Mater 4:1
17. Forero-Sandoval IY, Vega-Flick A, Alvarado-Gil JJ, Medina-Esquivel RA (2017) Study of thermal conductivity of magnetorheological fluids using the thermal-wave resonant cavity and its relationship with the viscosity. Smart Mater Struct 26:025010
18. Fu Y, Yao J, Zhao H et al (2018) Bidisperse magnetic particles coated with gelatin and graphite oxide: magnetorheology, dispersion stability, and the nanoparticle-enhancing effect. Nanomaterials 8:714
19. Ham JM, Homsy GM (1988) Hindered settling and hydrodynamic dispersion in quiescent sedimenting suspensions. Int J Multiph Flow 14:533–546
20. Jha S, Jain VK (2009) Rheological characterization of magnetorheological polishing fluid for MRAFF. Int J Adv Manuf Technol 42:656–668
21. Jiang W, Zhang Y, Xuan S et al (2011) Dimorphic magnetorheological fluid with improved rheological properties. J Magn Magn Mater 323:3246–3250
22. Jönkkäri I, Isakov M, Syrjälä S (2015) Sedimentation stability and rheological properties of ionic liquid–based bidisperse magnetorheological fluids. J Intell Mater Syst Struct 26:2256–2265
23. Kittipoomwong D, Klingenberg DJ, Ulicny JC (2005) Dynamic yield stress enhancement in bidisperse magnetorheological fluids. J Rheol (N Y N Y) 49:1521–1538
24. Kordonsky WI, Gorodkfn SP, Demchuk SA (1993) Magnetorheological control of heat transfer. Int J Heat Mass Transf 36:2783–2788
25. Krishna H, Kumar H, Gangadharan K (2017) Optimization of magneto-rheological damper for maximizing magnetic flux density in the fluid flow gap through fea and ga approaches. J Inst Eng Ser C 98:533–539
26. Kumar PM, Kumar J, Tamilarasan R et al (2015) Review on nanofluids theoretical thermal conductivity models. Eng J 19:67–83
27. Kwon SH, Jung HS, Choi HJ et al (2018) Effect of octahedral typed iron oxide particles on magnetorheological behavior of carbonyl iron dispersion. Colloids Surfaces A Physicochem Eng Asp 555:685–690. https://doi.org/10.1016/j.colsurfa.2018.07.060
28. Lee JY, Kwon SH, Choi HJ (2019) Magnetorheological characteristics of carbonyl iron microparticles with different shapes. Korea-Australia Rheol J 31:41–47
29. Leong KC, Yang C, Murshed SMS (2006) A model for the thermal conductivity of nanofluids - the effect of interfacial layer. J Nanoparticle Res 8:245–254. https://doi.org/10.1007/s11051-005-9018-9
30. Li Y, Luo Y, Wang Y et al (2021) Research on characterization method and influencing factors of sedimentation stability of magnetorheological fluid. Korea Aust Rheol J 33:309–320. https://doi.org/10.1007/s13367-021-0024-y
31. Liu YD, Lee J, Choi SB, Choi HJ (2013) Silica-coated carbonyl iron microsphere based magnetorheological fluid and its damping force characteristics. Smart Mater Struct. https://doi.org/10.1088/0964-1726/22/6/065022
32. López-López MT, Zugaldía A, González-Caballero F, Durán JDG (2006) Sedimentation and redispersion phenomena in iron-based magnetorheological fluids. J Rheol (N Y N Y) 50:543–560. https://doi.org/10.1122/1.2206716
33. Mangal SK, Kumar A (2014) Experimental and numerical studies of magnetorheological (MR) damper. Chinese J Eng 2014:1–7. https://doi.org/10.1155/2014/915694
34. Mangal SK, Kumar A (2015) Geometric parameter optimization of magneto-rheological damper using design of experiment technique. Int J Mech Mater Eng 10:1–9. https://doi.org/10.1186/s40712-015-0031-1
35. Mistik SI, Shah T, Hadimani RL, Siores E (2012) Compression and thermal conductivity characteristics of magnetorheological fluid-spacer fabric smart structures. J Intell Mater Syst Struct 23:1277–1283. https://doi.org/10.1177/1045389X12447295
36. Morillas JR, Bombard AJF, De Vicente J (2018) Enhancing magnetorheological effect using bimodal suspensions in the single-multidomain limit. Smart Mater Struct. https://doi.org/10.1088/1361-665X/aac8ae
37. Murshed SMS, De Castro CAN (2011) Contribution of Brownian motion in thermal conductivity of nanofluids. Proc World Congr Eng 3:1905–1909
38. Ngatu GT, Wereley NM (2007) Viscometric and sedimentation characterization of bidisperse magnetorheological fluids. IEEE Trans Magn 43:2474–2476. https://doi.org/10.1109/TMAG.2007.893867
39. Nguyen QH, Han YM, Choi SB, Wereley NM (2007) Geometry optimization of MR valves constrained in a specific volume using the finite element method. Smart Mater Struct 16:2242–2252. https://doi.org/10.1088/0964-1726/16/6/027
40. Nicolai H, Herzhaft B, Hinch EJ et al (1995) Particle velocity fluctuations and hydrodynamic self-diffusion of sedimenting non-Brownian spheres. Phys Fluids 7:12–23. https://doi.org/10.1063/1.868733
41. Piao SH, Bhaumik M, Maity A, Choi HJ (2015) Polyaniline/Fe composite nanofiber added softmagnetic carbonyl iron microsphere suspension and its magnetorheology. J Mater Chem C 3:1861–1868. https://doi.org/10.1039/c4tc02491e
42. Pisuwala MS, Upadhyay RV, Parekh K (2019) Contribution of magnetic nanoparticle in thermal conductivity of flake-shaped iron particles based magnetorheological (MR) fluid. J Appl Phys. https://doi.org/10.1063/1.5109021
43. Pu H, Jiang F (2005) Towards high sedimentation stability: magnetorheological fluids based on CNT/Fe3O4 nanocomposites. Nanotechnology 16:1486–1489. https://doi.org/10.1088/0957-4484/16/9/012
44. Reinecke BN, Shan JW, Suabedissen KK, Cherkasova AS (2008) On the anisotropic thermal conductivity of magnetorheological suspensions. J Appl Phys. https://doi.org/10.1063/1.2949266
45. Richardson JF, Zaki WN (1997) Sedimentation and fluidisation: Part I. Chem Eng Res Des 75:S82–S100. https://doi.org/10.1016/s0263-8762(97)80006-8
46. Sarkar C, Hirani H (2015) Effect of particle size on shear stress of magnetorheological fluids. Smart Sci 3:65–73. https://doi.org/10.1080/23080477.2015.11665638

47. Sassi S, Cherif K, Mezghani L et al (2005) An innovative magnetorheological damper for automotive suspension: from design to experimental characterization. Smart Mater Struct 14:811–822. https://doi.org/10.1088/0964-1726/14/4/041
48. Sedlacik M, Pavlinek V, Lehocky M et al (2011) Plasma-treated carbonyl iron particles as a dispersed phase in magnetorheological fluids. Colloids Surfaces A Physicochem Eng Asp 387:99–103. https://doi.org/10.1016/j.colsurfa.2011.07.035
49. Shah K, Phu DX, Seong MS et al (2014) A low sedimentation magnetorheological fluid based on plate-like iron particles, and verification using a damper test. Smart Mater Struct. https://doi.org/10.1088/0964-1726/23/2/027001
50. Shivaram AC, Gangadharan KV (2007) Statistical modeling of a magneto-rheological fluid damper using the design of experiments approach. Smart Mater Struct 16:1310–1314. https://doi.org/10.1088/0964-1726/16/4/044
51. Steinour HH (1944) Rate of Sedimentation. Ind Eng Chem 36:840–847. https://doi.org/10.1021/ie50417a018
52. Wang X, Gordaninejad F (2006) Study of magnetorheological fluids at high shear rates. Rheol Acta 45:899–908. https://doi.org/10.1007/s00397-005-0058-y
53. Wong PL, Bullough WA, Feng C, Lingard S (2001) Tribological performance of a magneto-rheological suspension. Wear 247:33–40. https://doi.org/10.1016/S0043-1648(00)00507-X
54. Xu ZD, Guo WY, Chen BB (2015) Preparation, property tests, and limited chain model of magnetorheological fluid. J Mater Civ Eng 27:1–10. https://doi.org/10.1061/(ASCE)MT.1943-5533.0001190
55. Xue Q, Xu WM (2005) A model of thermal conductivity of nanofluids with interfacial shells. Mater Chem Phys 90:298–301. https://doi.org/10.1016/j.matchemphys.2004.05.029
56. Zhang WL, Liu YD, Choi HJ (2012) Field-responsive smart composite particle suspension: materials and rheology. Korea Aust Rheol J 24:147–153
57. Zhang Y, Li D, Zhang Z (2019) The study of magnetorheological fluids sedimentation behaviors based on volume fraction of magnetic particles and the mass fraction of surfactants. Mater. Res. Express 6:126127